Electronic Supplementary Material (ESI) for Journal of Materials Chemistry B.

Supporting Information

Fast Detection of *Staphylococcus aureus* using thiol-Functionalized WS_2 Quantum Dots and Bi_2O_2Se Nanosheets Hybrid Through Fluorescence Recovery Mechanism

Abdul Kaium Mia[1], Abhilasha Bora[1], Md Tarik Hossain[2], Swapnil Sinha[3], P. K. Giri[*1,2]

[1]Centre for Nanotechnology, Indian Institute of Technology Guwahati, Guwahati 781039, India

[2]Department of Physics, Indian Institute of Technology Guwahati, Guwahati 781039, India

[3]BioNEST, Indian Institute of Technology Guwahati, Guwahati 781039, India

1. Synthesis of WS_2 QDs:

The schematic representations of the synthesis of WS_2 QDs are shown in Figure S1. High-energy pulses from Tip sonicator break the WS_2 sheets and form small QDs during probe sonication. The functional groups in NMP help in layer intercalations and dispersions of QDs. With 5 hours of probe sonication,

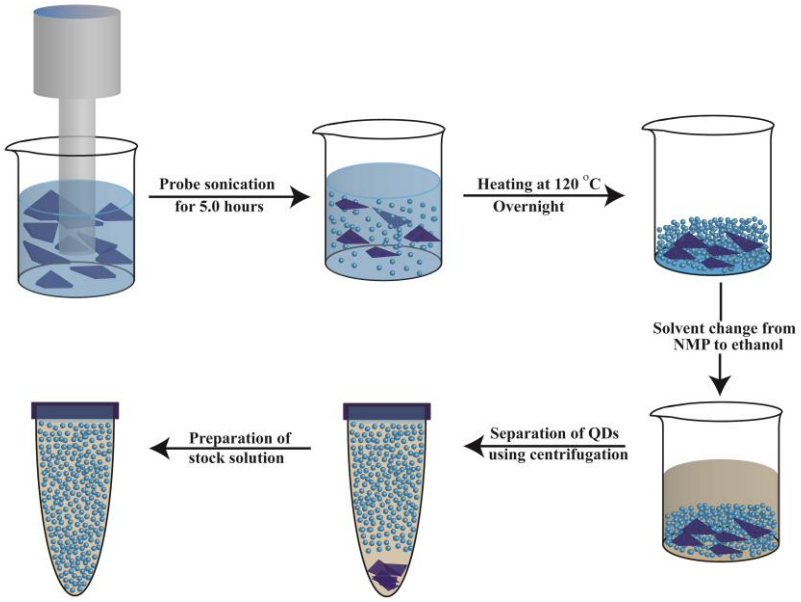

Figure S1: Schematics illustration of the synthesis of WS_2 QDs from bulk WS_2 powder using probe sonication.

* Corresponding author; email: giri@iitg.ac.in

the solution has a mixture of QDs and WS_2 NSs. After sonication, the solution was kept on a hot plate at 120 °C overnight to remove NMP. Finally, a known weight of the product was mixed in ethanol and centrifuged at 12000 rpm at 4 °C to separate the QDs and NSs. The supernatant contains QDs, while the bottom comprises NSs and other bulk products. The concentration of the stock solution was measured by knowing the amount of dry QDs mixture added and the amount recovered after centrifugation.

2. ssDNA Aptamer selection

The ssDNA Aptamer specifically identifying and binding to *S. aureus* was developed by using the Cell-SELEX (Systematic Evolution of Ligands by EXponential enrichment) technology[1,2]. Briefly, 1.5µM ssDNA Aptamer library was incubated with 10^8 CFU/mL (Colony Formation Unit/mL) of *S. aureus* suspended in 1-X phosphate buffered saline (PBS) at room temperature. After 45 min, cells were centrifuged for 5 min at 8000 rpm and the unbound ssDNA Aptamers in aqueous phase were discarded and the cell bound aptamers were re-suspended in 250µl nuclease free deionized water. The cell-bound selected aptamers were recovered by heating the suspension at 95ºC for 10 min followed by centrifugation at 12,000 rpm for 15 min. The selected aptamer pool was enriched by Polymerase Chain reaction (PCR) being carried out for 10 cycles using 0.15µM of Forward primer [5'-GGCTGGATGGGGCGTGT-3'] and 0.15µM 5'-Biotin-labeled reverse primer [5'-CGCTGTCCGCACCGTTG-3']. The PCR program used was: pre-denaturation at 95ºC, 5 min, followed by cycling step; 95ºC for 20s, annealing at 55ºC for 5s and extension at 72ºC for 10s. Amplified 2µg of dsDNA pool was immobilized on activated streptavidin magnetic beads (NEB) in 200µl of binding buffer (10mM Tris-HCl pH8.0, 1mM EDTA pH8.0, 2M NaCl). The selected ssDNA aptamer strand was separated from biotinylated strand by alkaline denaturation using 500µl of 10mM NaOH followed by purification by NAP-5 (Cytiva) desalting column according to manufactures' instructions. Before using the purified ssDNA for next round, the ssDNA pool was concentrated to the volume of ~150µl. The SELEX was carried out for 10 rounds. For specificity to target S. aureus, after SELEX rounds 4, 6 and 8, negative selection was carried out using non-target bacterial: E. coli, E.faecalis, K. pneumoniae, Pseudomonas sp. and Proteus sp. During negative selection rounds, bound

ssDNA aptamer pool was incubated with non-target bacteria pool for 30 min and unbound ssDNA pool was recovered by centrifugation and immediately incubated with target S. aureus. After the last round of selection, the ssDNA Aptamer pool was PCR amplified using unlabeled forward and reverse primers, purified and cloned into the TA-cloning vector using pGEM-T® easy vector systems (Promega), transformed in JM109 competent cells and plated on IPTG-Xgal-Amp-LB Agar plates. Positive bacterial colonies (white colonies) were inoculated in 5 ml of Luria Bertani (LB) media and grown overnight at 37ºC at 220 rpm. Plasmids were isolated and individual cloned DNA Aptamers were DNA sequenced using Sangers dideoxy chain termination method (1st Base, Axil Scientific, Singapore facility). The 20 selected DNA Aptamers that were sequenced, 3 of them were repeated and thus these 3 Aptamers were individually synthesized commercially with FAM label at 5'-end (IDT DNA Technologies, USA). Flow cytometry was used to assess the binding of the individual aptamer to target S. *aureus* and determination of dissociation constants (K_d) of individual selected Aptamers with target S. *aureus*. The Aptamer used in the present work exhibited highest specificity to the target S. *aureus* with K_d value of 40.96nM. The evaluated *S. aureus* Aptamer was commercially synthesized (IDT DNA Technologies, USA) with thiol group modification at the 5'-end of the DNA molecule; 5´-ThioMC6-D-GGC TGG ATG GGG CGT GTT GAT TCG AGT CGG AGA CGG CAT CCT GCA CAA ATG CCA ACG GTG CGG ACA GCG-3´.

3. **Elemental composition of Bi_2O_2Se:**

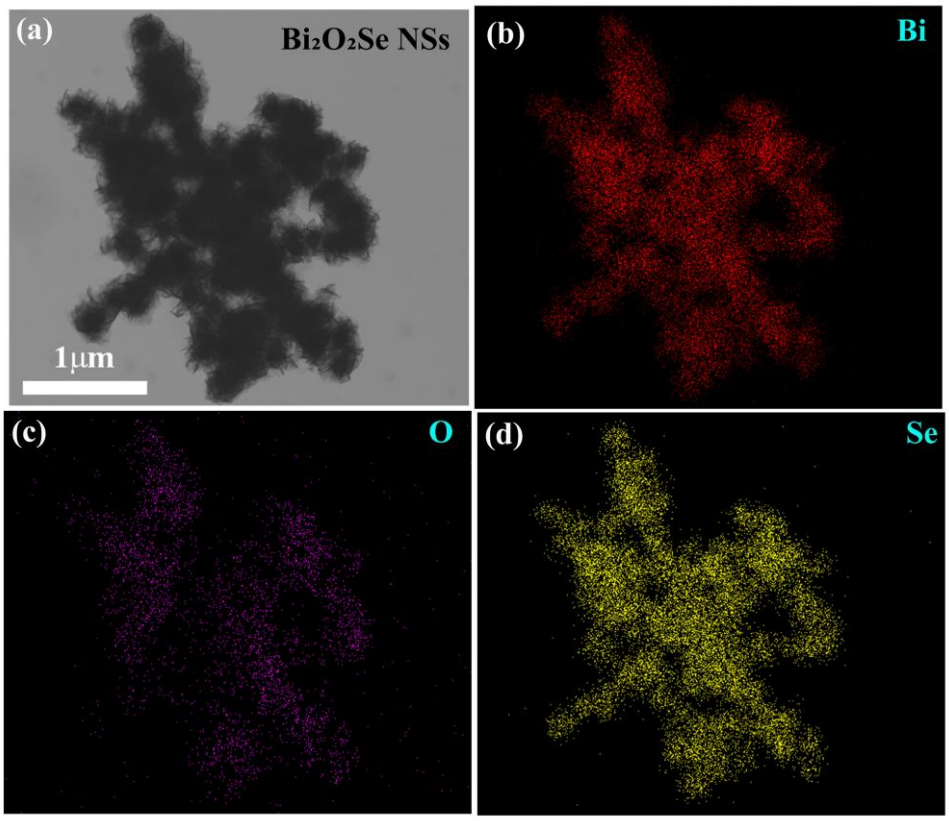

Figure S2: Bright-field TEM image of Bi_2O_2Se NS. (b-d) The corresponding STEM elemental mapping of Bi, O, and Se.

The elemental composition of synthesized Bi_2O_2Se was calculated from the energy-dispersive X-ray spectroscopy (EDS) of the Bi_2O_2Se NSs using a scanning transmission electron microscope (STEM; JEM 2100F, 200 kV) and is shown in Figure S2.

4. XPS survey spectra:

The XPS survey scan spectrum for WS_2 QDs, Aptamer functionalized WS_2 QDs, Bi_2O_2Se NSs and WS_2 QDs/Bi_2O_2Se NSs composite are shown in Figure S3. For WS_2 QDs, we can see a clear signature of elements tungsten and sulfur. Additionally, we have observed a strong peak at 400 eV corresponding to nitrogen species arising from solvent. In case of aptamer functionalized WS_2 QDs, additional one peak is observed at 133 eV corresponding to phosphorus as labelled in figure S3, as well as the increase in nitrogen peak strength, as the aptamers also contains nitrogen. Bi_2O_2Se NSs survey spectra shows

many peaks mainly originated form bismuth, all the peaks are labelled from previous reports[3,4]. Finally, for the WS_2 QDs/Bi_2O_2Se NSs composite, the broad peak around 160 eV contains sulfur and bismuth.

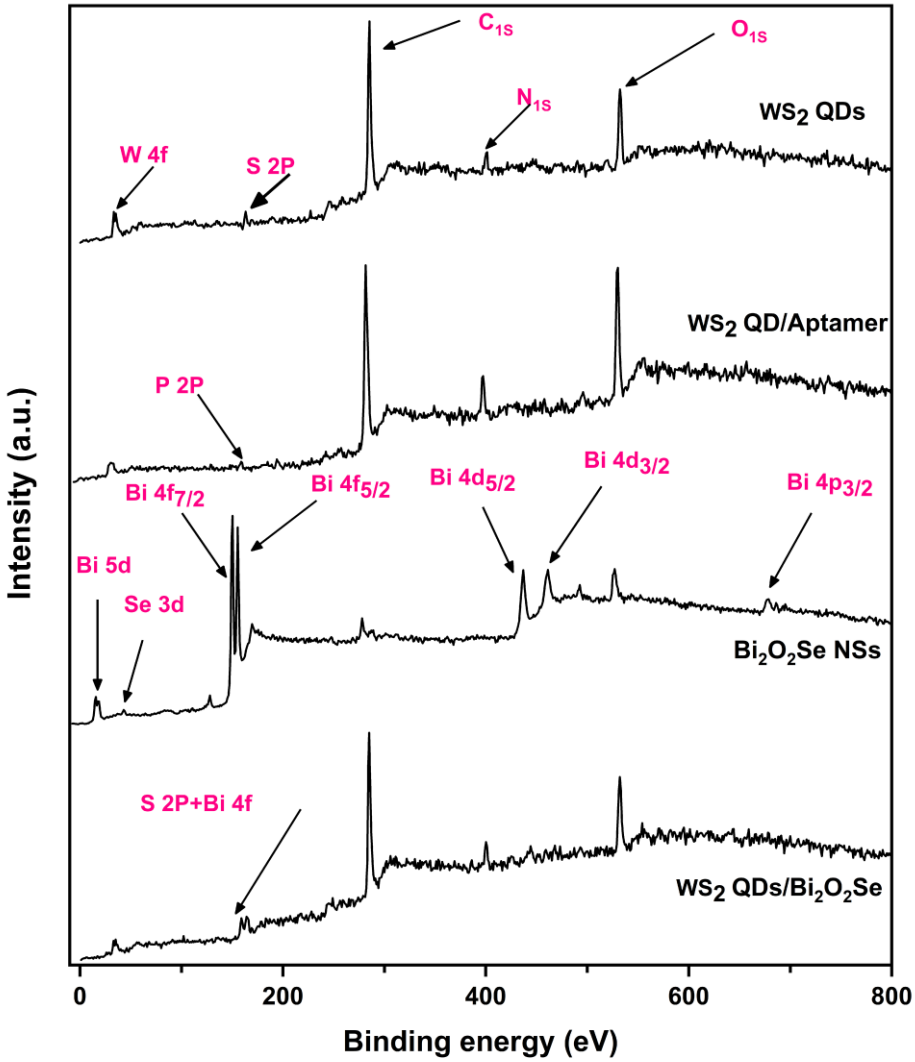

Figure S3: The XPS survey scan spectra of WS_2 QDs, WS_2 QDs/Bi_2O_2Se NSs composite and aptamer functionalized WS_2 QDs.

5. XPS spectra of functionalized WS_2 QDs:

High resolution core binding energes for sulfur and tungsten of aptamer functionalized WS_2 QDs are shown in figure S4. In addition to the S^{2-} oxidation state of sulfur, the other two peaks as labelled by 1 and 2 are due to defects and sulfur vacancy sites[5–7].

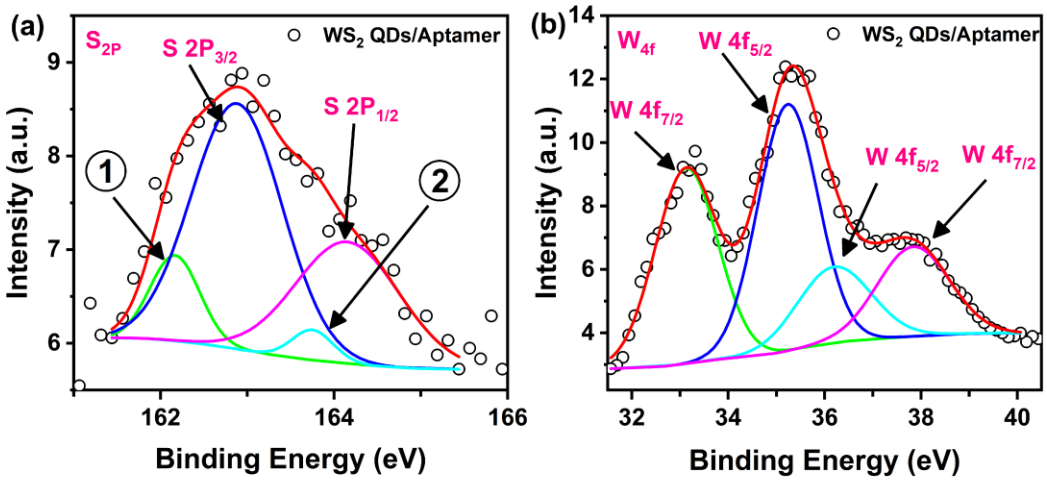

Figure S4: XPS Core level binding energy spectra with fitting for aptamer functionalized WS_2 QDs (a) sulfur 2P (b) tungsten 4f.

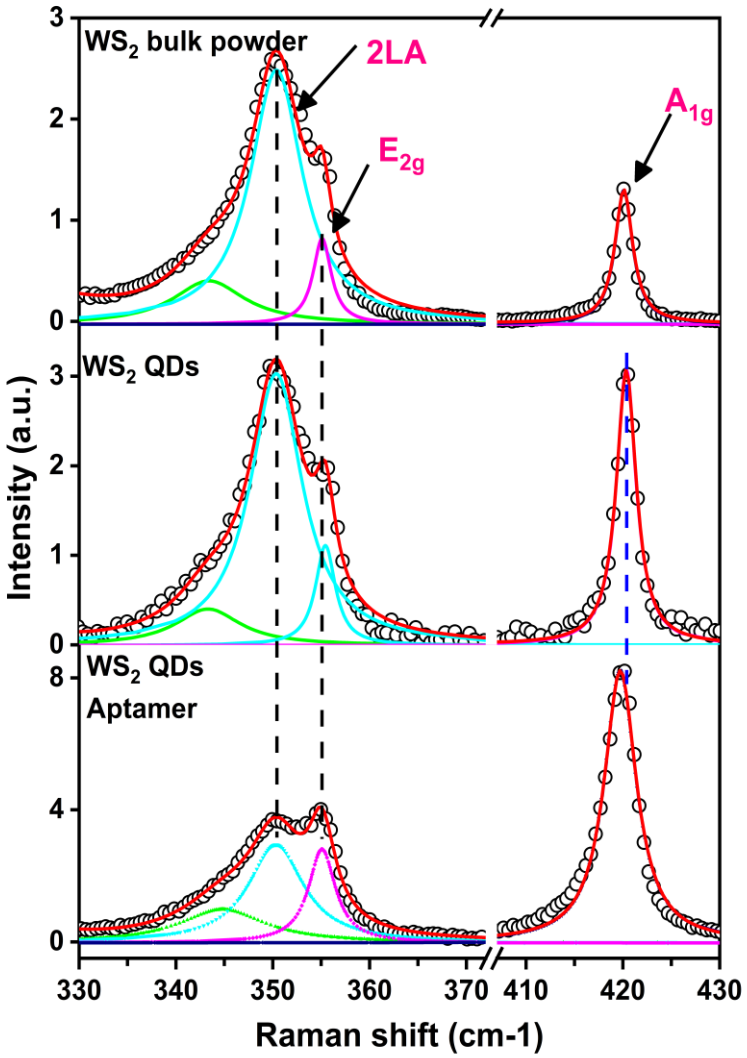

Figure S5: Fitted Raman spectrum for WS_2 bulk powder, WS_2 QDs and Aptamer functionalized WS_2 QDs (from top to bottom).

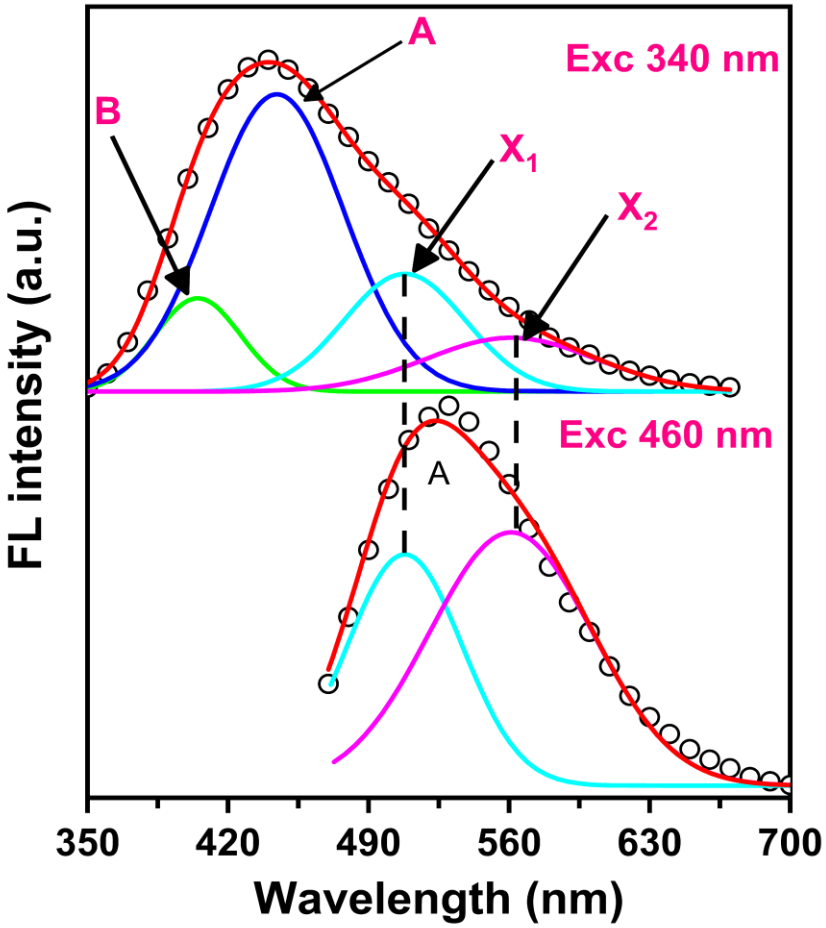

Figure S6: The exciton wavelength dependent FL emission spectra of WS_2 QDs and its fitting.

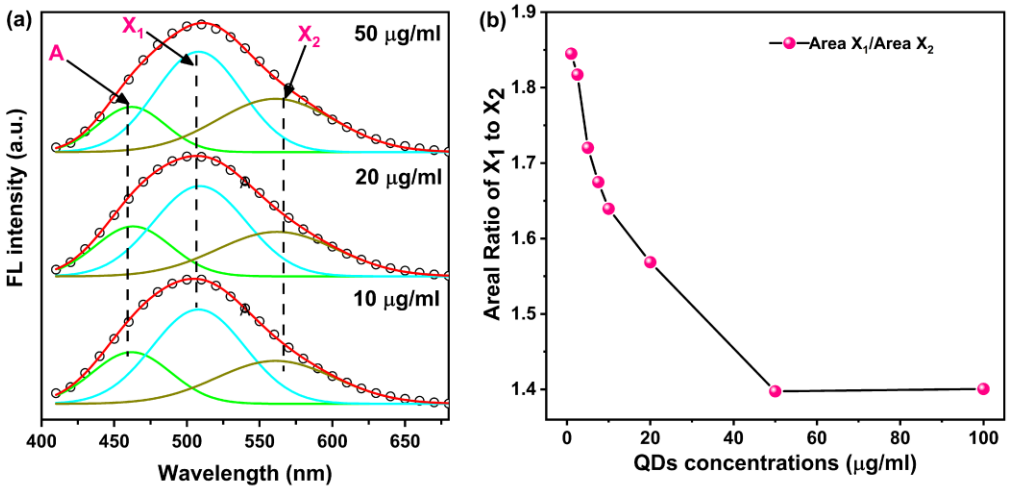

Figure S7: (a) Concentration-dependent FL emission spectra and its fitting for WS_2 QDs; at higher concentration the defect bound exciton peak (X_2) is dominant. (b) Areal intensity ratio of X_1 to X_2 as a function of QD concentrations.

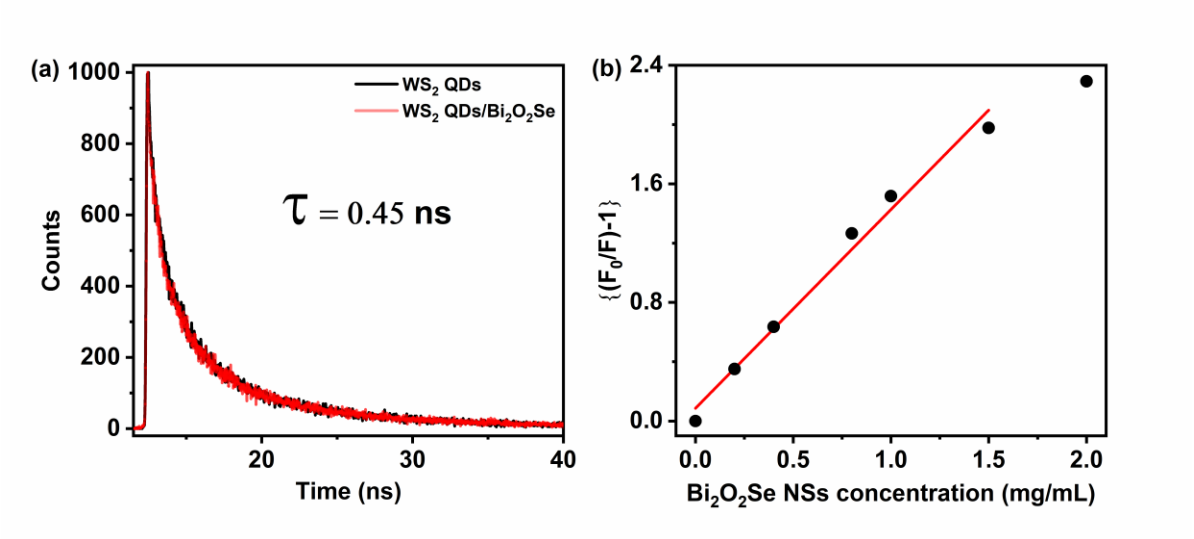

Figure S8: (a)Comparison of TRPL spectra of WS_2 QDs and WS_2/Bi2O2Se NSs composite, (b) Stern–Volmer plot for FL quenching showing linear behavior.

In Figure S9, we show the variation of composite FL emission intensity with time. This shows that the FL intensity remains almost constant after Bi_2O_2Se addition up to 7 minutes and slightly increases afterward. However, this increase is much smaller than the restoration of FL intensity in the presence of *S. aureus* bacteria.

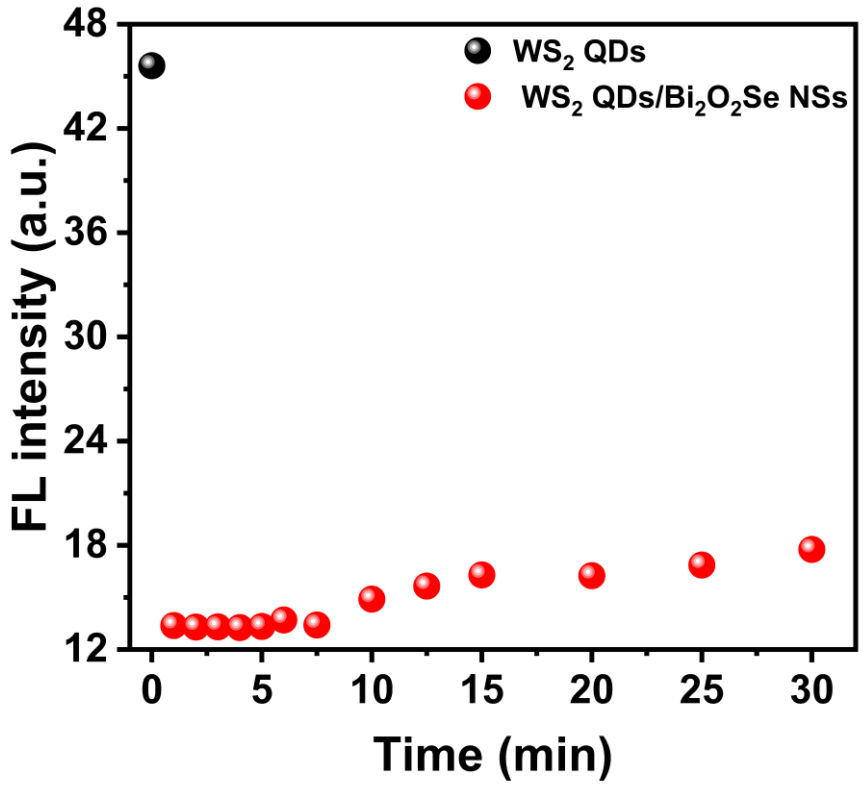

Figure S9: The variation of FL emission intensity of WS_2 QDs/Bi_2O_2Se composite with time.

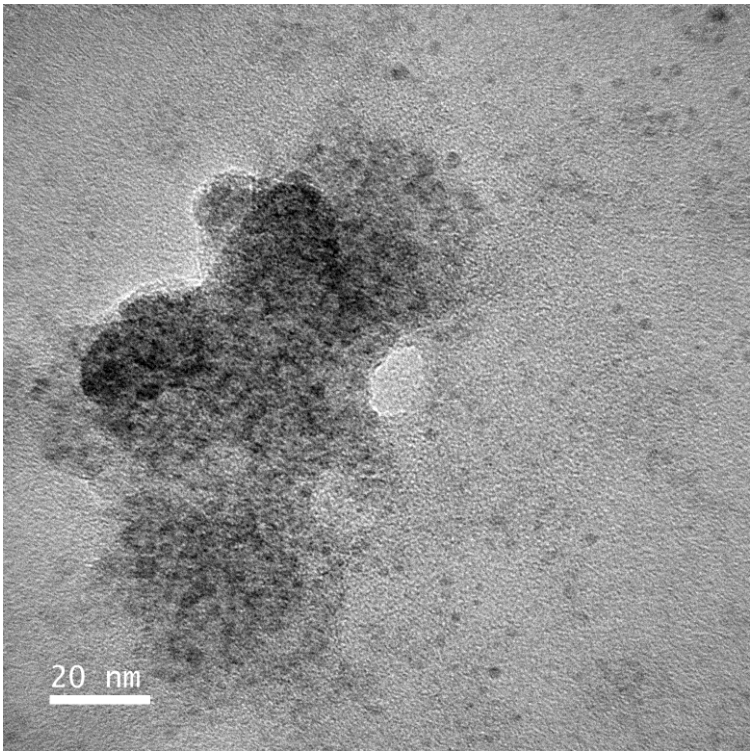

Figure S10: FETEM image of WS2 QDs after the addition of bacteria. QDs can be clearly seen outside the Bi_2O_2Se NSs.

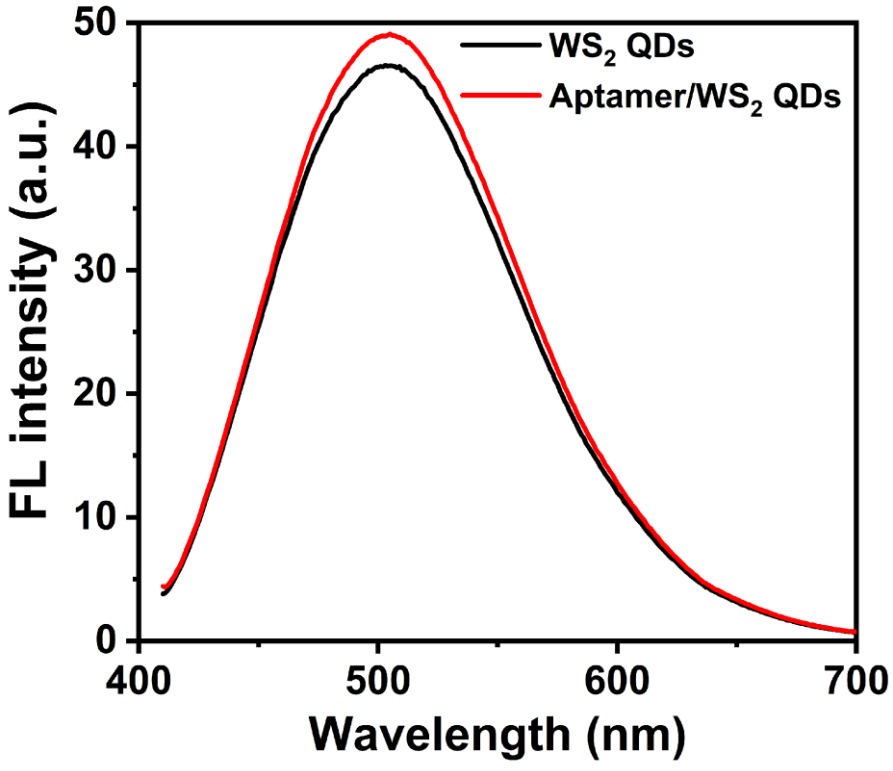

Figure S11: (a) The effect of aptamer in WS_2 QDs FL emission.

Functionalization effect on WS2 QDs FL emission:

The thiol functional covalently attaches to the sulfur vacancy sites of the WS_2 QDs and hence reduces the sulfur vacancy concentration. The effect of aptamer functionalization on the WS_2 QDs FL emission intensity is shown in figure S11. It was observed that the intensity is increased marginally by 5.6% only. This enhancement of the FL intensity can be attributed to the passivation of sulfur vacancies by thiol functional groups, which was already observed in Raman and XPS spectroscopy.

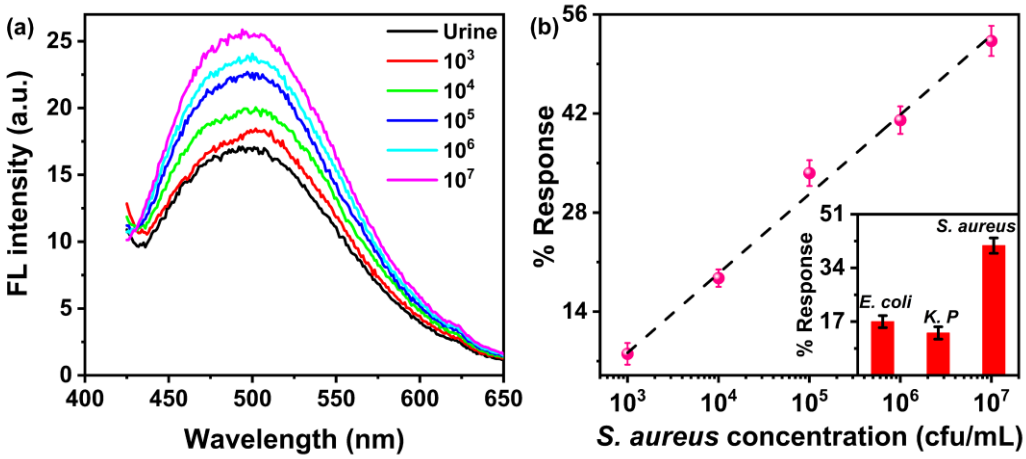

Figure S12: (a) FL emission of the system at different concentration of S. aureus in urine medium. (b) Calibration curve for urine medium with S. aureus concentration, the inset shows the selectivity data in urine medium.

Table S1: Summary of the performance of different sensors for detecting S. Aureus.

Material and methods	Linear range Cfu/ml	Lower detection limt (cfu/ml)	Response Time (minutes)	Reference
Electrochemical	8×10^2 to 1×10^3	800	02	Reference [8]
Colorimetric	1.5×10^2 to 1.5×10^6	1.500	40	Reference [9]
Fluorimetric Assay	1×10^3 to 1×10^9	2.900	130	Reference [10]
Long-period fiber gratings	1×10^4 to 1×10^8	224	30	Reference [11]
Fiber biosensor	7×10^1 to 7×10^4	3.1	40	Reference [12]
Electrochemical	3×10^0 to 3×10^7	3.0	30	Reference [13]
Fluorescence	10^0 to 10^7	1	240	Reference [14]
Fluorescence	10^1 to 10^7	11.12	120	Reference [15]
Polymerase chain reaction	1.8×10^1 to 1.8×10^6	18	240	Reference [16]
Fluorescence	10^3 to 10^7	850	15	*This work*

1. Fluorescence quantum yield measurement:

Fluorescence quantum yield (FLQY) was measured following the instructions in the operational manual of the instrument (FM-SPHERE, Horiba with Horiba Jobin Yvon, Fluoromax-4). The given relation was used to evaluate the FLQY:

$$FLQY = \frac{E_C - E_A}{L_A - L_C} \times 100\%$$

In the case of our WS_2 QDs under 330 nm excitation

L_C=34950 ; L_A=943696 ; E_C= 655889 ; and E_A=182325

$$FLQY = \frac{655889 - 182325}{943696 - 34950} \times 100\% = 52.1\ \%$$

Here, E_C is the integrated luminescence of the sample (WS_2 QDs in solution) caused by direct excitation, E_A is the integrated luminescence from the solvent ethanol, L_C is the integrated excitation profile when the sample is directly excited by the incident beam and L_A is the integrated excitation profile from the solvent. First of all, the integrating sphere was calibrated by measuring the FLQY of the standard samples (Quinine sulfate, Rhodamine 101). Then, before measuring, the excitation (at 330 nm) intensity with a blank integrating sphere was adjusted to ~10^6 counts by regulating the slit and neutral density filter. The solvent was placed in the liquid sample holder inside the integrating sphere, and its integrated excitation profile (L_A) and integrated luminescence (E_A) were recorded. Next, the sample was placed inside the integrating sphere in the liquid sample holder. Similarly, the integrated excitation profile with the sample (L_C) and integrated luminescence of the sample (E_C) was obtained and corrected using the instrument correction file. Finally, we determined the FLQY of the WS_2 QDs from the instrument software.

References

1 K. Sefah, D. Shangguan, X. Xiong, M. B. O'Donoghue and W. Tan, *Nat Protoc*, 2010, **5**, 1169–1185.
2 D. Yılmaz, T. Muslu, A. Parlar, H. Kurt and M. Yüce, *Journal of Biotechnology*, 2022, **354**, 10–20.
3 U. Khan, Y. Luo, L. Tang, C. Teng, J. Liu, B. Liu and H.-M. Cheng, *Advanced Functional Materials*, 2019, **29**, 1807979.
4 J.-L. Jiang, S.-T. Dong, Z. Fu, M.-C. Yu, L. Zhao and L. Wang, *Metals*, 2022, **12**, 1881.
5 M. Donarelli, F. Bisti, F. Perrozzi and L. Ottaviano, *Chemical Physics Letters*, 2013, **588**, 198–202.
6 M. Donarelli, S. Prezioso, F. Perrozzi, F. Bisti, M. Nardone, L. Giancaterini, C. Cantalini and L. Ottaviano, *Sensors and Actuators B: Chemical*, 2015, **207**, 602–613.
7 A. Bora, L. P. L. Mawlong, R. Das and P. K. Giri, *Journal of Colloid and Interface Science*, 2020, **561**, 519–532.
8 G. A. Zelada-Guillén, J. L. Sebastián-Avila, P. Blondeau, J. Riu and F. X. Rius, *Biosensors and Bioelectronics*, 2012, **31**, 226–232.
9 Y. J. Sung, H.-J. Suk, H. Y. Sung, T. Li, H. Poo and M.-G. Kim, *Biosensors and Bioelectronics*, 2013, **43**, 432–439.
10 W. Kong, J. Xiong, H. Yue and Z. Fu, *Anal. Chem.*, 2015, **87**, 9864–9868.
11 F. Yang, T.-L. Chang, T. Liu, D. Wu, H. Du, J. Liang and F. Tian, *Biosensors and Bioelectronics*, 2019, **133**, 147–153.
12 L. Chen, Y.-K. Leng, B. Liu, J. Liu, S.-P. Wan, T. Wu, J. Yuan, L. Shao, G. Gu, Y. Q. Fu, H. Xu, Y. Xiong, X.-D. He and Q. Wu, *Sensors and Actuators B: Chemical*, 2020, **320**, 128283.
13 U. Farooq, M. W. Ullah, Q. Yang, A. Aziz, J. Xu, L. Zhou and S. Wang, *Biosensors and Bioelectronics*, 2020, **157**, 112163.
14 J. Zhou, L. Yin, Y. Dong, L. Peng, G. Liu, S. Man and L. Ma, *Analytica Chimica Acta*, 2020, **1127**, 225–233.
15 Y. Guo, J. Li, X. Song, K. Xu, J. Wang and C. Zhao, *ACS Appl. Bio Mater.*, 2021, **4**, 420–427.
16 M. Deng, Y. Wang, G. Chen, J. Liu, Z. Wang and H. Xu, *Journal of Dairy Science*, 2021, **104**, 12342–12352.